RESEARCH ARTICLE | APRIL 13 2023

Entropy driven disorder–order transition of a metal–organic framework with frustrated flexibility

Special Collection: Challenges and Perspectives in Materials Chemistry—A Celebration of Prof. Sir Anthony K. Cheetham's 75th Birthday

Roman Pallach; Jan-Benedikt Weiß; Katrin Vollmari; ... et. al

APL Mater 11, 041118 (2023)
https://doi.org/10.1063/5.0144718

Entropy driven disorder–order transition of a metal–organic framework with frustrated flexibility

Cite as: APL Mater. 11, 041118 (2023); doi: 10.1063/5.0144718
Submitted: 31 January 2023 • Accepted: 29 March 2023 •
Published Online: 13 April 2023

Roman Pallach, Jan-Benedikt Weiß, Katrin Vollmari, and Sebastian Henke[a)]

AFFILIATIONS

[1]Anorganische Chemie, Fakultät für Chemie und Chemische Biologie, Technische Universität Dortmund, Otto-Hahn-Straße 6, 44227 Dortmund, Germany

Note: This paper is part of the Special Topic on Challenges and Perspectives in Materials Chemistry - A Celebration of Professor Sir Anthony K. Cheetham's 75th Birthday.

[a)]**Author to whom correspondence should be addressed:** sebastian.henke@tu-dortmund.de

ABSTRACT

Flexible metal–organic frameworks (MOFs), showing a reversible phase change behavior in response to guest adsorption or temperature, provide unique opportunities for molecular separation or energy storage applications. Herein, we investigate the complex guest- and temperature-responsive behavior of a functionalized MOF-5 derivative. The material is characterized by a geometrically rigid network structure that is decorated with dispersion energy donating hexyloxy substituents. Distinguished by the phenomenon of frustrated flexibility, the functionalized MOF-5 derivative switches between a highly crystalline, cubic structure and a semi-crystalline, aperiodically distorted structure depending on guest adsorption and temperature. Via a combination of several variable temperature global and local structure techniques (x-ray diffraction, x-ray total scattering, and Fourier-transform IR spectroscopy), detailed insights into the complementary disorder–order transitions of the framework backbone and the dangling hexyloxy substituents are provided. Our results set the stage for the discovery of new responsive MOFs exhibiting a more complex phase change behavior interfacing periodic and aperiodic structural changes.

INTRODUCTION

The investigation of functional materials, which change their physical properties depending on external triggers, is of ongoing interest for various fields of materials research. Metal–organic frameworks (MOFs) are porous coordination polymers constructed of inorganic building units (e.g., metal ions and metal-oxo-clusters) joined by organic linkers.[1,2] A particularly fascinating subclass is flexible MOFs,[3] which undergo structural changes as a function of external stimuli, such as changes in temperature[4] or mechanical pressure,[5,6] guest uptake,[7,8] light irradiation,[9] or electric fields.[10,11] Their unique properties render these materials interesting for applications in the fields of gas storage,[12] separations,[13] chemical sensing,[14,15] or as shock absorbers.[16]

Despite being typically associated with perfectly ordered and crystalline structures, there is growing interest in non-crystalline MOFs and those featuring extensive disorder.[17–24] In particular, for meltable MOFs, their glassy state offers exciting properties, such as isotropy, mechanical robustness, and the absence of grain boundaries, which are advantageous for ionic conductivity or processability, for example.[25–28] Moreover, despite sometimes being very similar in chemical composition, non-crystalline and highly disordered MOFs may exhibit fundamentally different properties from their crystalline counterparts in the fields of catalysis,[29–31] gas separation,[32,33] or drug release.[34,35] Naturally, due to the lack of long-range order, such materials are more difficult to characterize than their crystalline counterparts. In particular, responsive MOFs, switching between crystalline and non- or semi-crystalline states depending on the environment or external triggers, are reported only rarely.[36,37] The understanding of such a kind of unusual crystalline-to-non-crystalline phase change behavior, however, lays the foundation

for the application of these stimuli-responsive materials in various fields.

Recently, we have introduced the new concept of *frustrated flexibility*.[38] It is based on a rigid and non-responsive MOF structure type that does not allow concerted hinging movements of its building units.[39,40] Decoration of the organic building units with dispersion energy donors (DEDs), such as alkoxy groups, however, changes the free energy landscape of the MOF so that a contraction of the framework, aided by intra-framework dispersion interactions, becomes energetically favored after the removal of guest molecules. Due to competing forces between the attractive interactions of the DEDs, facilitating a contraction of the framework to a denser phase, and the geometric constraints of the framework backbone, requiring persistence of the open phase, the MOF enters a state of frustration. We demonstrated this concept for an isoreticular series of alkoxy-functionalized MOF-5-based compounds, denoted MOF-5-**CX** (Zn_4O(**CX**-bdc)$_3$ [Fig. 1(a), **CX**-bdc^{2-} = 2,5-dialkoxy-1,4-benzenedicarboxylate)] with **X** = 2–7.[41] The T_d symmetry of the $Zn_4O(O_2C)_6$ building units of these cubic frameworks is known to impede the hinging movements of the organic linkers typical for framework flexibility.[39,40] Nevertheless, the MOF-5-**CX** materials exhibit reversible guest-induced displacive structural transformations [Fig. 1(b)]. MOF-5-**C7**, the derivative with long heptyloxy substituents, switches between an expanded guest-filled cubic phase and a slightly contracted guest-free rhombohedral phase. The volume change when transitioning from the cubic to the rhombohedral phase amounts to −3% and comes along with slight distortions of the $[Zn_4O(O_2C)_6]$ building units. Shorter alkoxy substituents (MOF-5-**C6** to MOF-5-**C2**) yield stronger framework contractions between about −6% (**C6**) and −17% (**C2**) following guest removal. The volumetric contraction of the materials of the dried phases has been approximated based on powder x-ray diffraction (PXRD) data.[38] The stronger contraction mediated by the DEDs requires aperiodic distortions of the $[Zn_4O(O_2C)_6]$ building units, yielding a semi- or non-crystalline state, which, however, retains the topology (i.e., the connectivity pattern) of the framework.

A particularly exciting derivative of this series of materials is MOF-5-**C6**, which is on the edge between the cubic-to-rhombohedral and the cubic-to-semi-/non-crystalline transformation regimes. While the *N,N*-dimethylformamide (DMF) containing as-synthesized phase *as*-MOF-5-**C6** features a cubic structure with $Pm\bar{3}m$ symmetry, the guest-free *dry*-MOF-5-**C6** phase ($\Delta V \approx -6\%$ relative to *as*-MOF-5-**C6**) exhibits poor long-range order and very broad Bragg peaks in the PXRD pattern (Fig. 2).[38] Despite the structural contraction, *dry*-MOF-5-**C6** still features significant microporosity, which is accessible to CO_2 at 195 K but inaccessible to N_2 at 77 K.[38] Upon resolvation with DMF or even *n*-octane (*oct*-MOF-5-**C6**), the material returns to a highly crystalline cubic structure. The responsive nature of MOF-5-**C6** gives rise to highly unusual properties, such as continuous transformation from the semi-crystalline to the crystalline phase driven not only by the adsorption of guest molecules (driving force: enthalpy) but also by

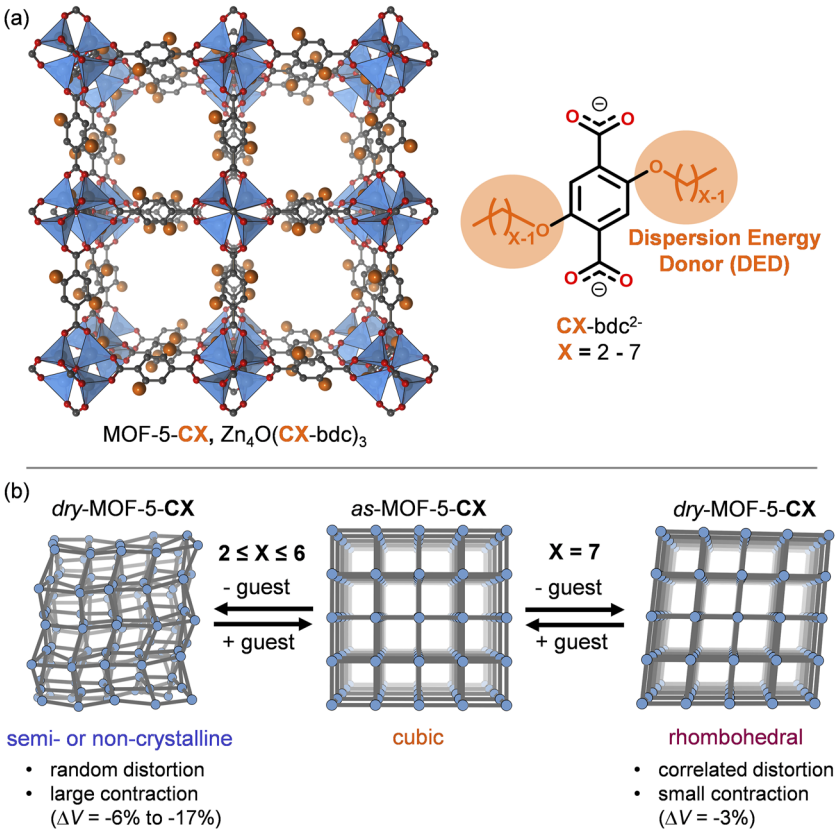

FIG. 1. (a) Illustration of the structure of the alkoxy-DED-functionalized MOF-5-**CX** derivatives and the implemented **CX**-bdc^{2-} linkers. Zn, O, and C atoms are shown in blue, red, and gray, respectively. H atoms are omitted. Coordination polyhedra around the Zn atoms are shown. The idealized positions of the DEDs are displayed as orange spheres. (b) Schematic representation of the alkoxy chain length-depending structural behavior of the MOF-5-**CX** derivatives as a function of guest content. The blue spheres illustrate the positions of the $[Zn_4O]^{6+}$ clusters, and the gray rods represent the position of the **CX**-bdc^{2-} linkers. The figure has been adapted from Ref. 38.

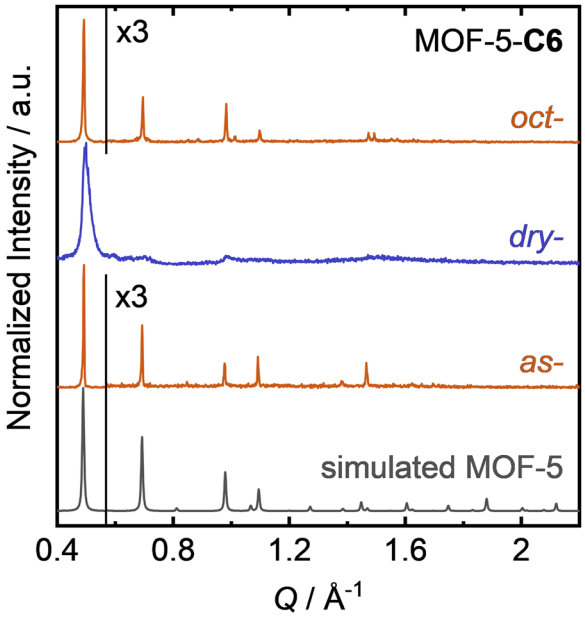

FIG. 2. PXRD patterns of MOF-5-**C6** in its DMF-solvated as-synthesized (*as*), guest-free (*dry*), and *n*-octane-solvated (*oct*) phases in comparison with the PXRD pattern of guest-free MOF-5. Data are taken from Ref. 38.

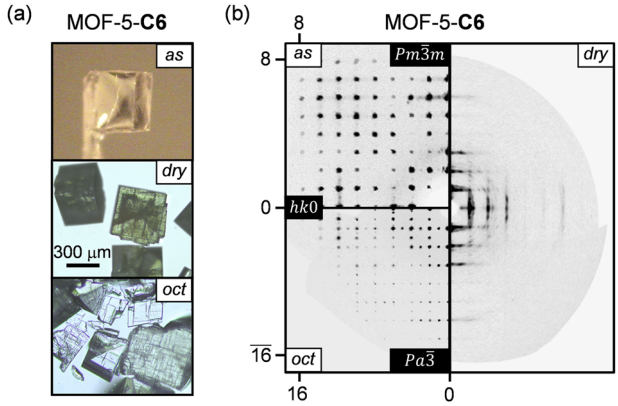

FIG. 3. (a) Microscopy images of the crystals and (b) excerpts of reconstructed reciprocal space maps of the (*hk*0) plane from single-crystal x-ray diffraction data of as-synthesized (*as*), guest-free (*dry*), and *n*-octane-resolvated (*oct*) MOF-5-**C6**. The scale bar in panel (a) applies to all images. The crystal structures corresponding to the x-ray diffraction data used for the generation of the reciprocal space maps were already published in Ref. 38.

temperature (driving force: entropy). The latter transformation is characterized by a strong increase in Bragg scattering intensity from the material with increasing temperature along with a marked sharpening of the scattering peaks and shifting of the peaks to lower angles. We postulated that this behavior arises from thermal vibrations of the alkoxy sidechains, which entropically outbalance the enthalpic stabilization of the contracted aperiodic semi-crystalline state at elevated temperatures. Thus, an increase in temperature leads to increased order of the framework backbone compensated by increased disorder of the DEDs. However, experimental evidence for this hypothesis is lacking so far.

In this work, we investigate the structural behavior of MOF-5-**C6** in detail by, first, revisiting the crystalline structure of the *n*-octane-filled *oct*-MOF-5-**C6** phase and providing new insights into the aperiodically distorted structure of the semi-crystalline *dry*-MOF-**C6** phase. Second, we investigate the mechanism of the unprecedented disorder–order transition of the guest-free *dry*-MOF-5-**C6** as a function of temperature by re-evaluating previously published *in situ* variable temperature (VT) PXRD data. Additional VT x-ray total scattering experiments and the corresponding x-ray pair distribution functions (XPDFs) together with VT Fourier-transform (FT)IR spectroscopy data shed light on the microscopic mechanisms underlying the extraordinary phase change behavior of this responsive framework material.

RESULTS AND DISCUSSION

Guest-responsive structural behavior

The guest-responsive structural transformations of MOF-5-**C6** are traceable on the single-crystal level [Fig. 3(a)]. The DMF-filled as-synthesized crystals of *as*-MOF-5-**C6** are transparent cubic crystals with sizes up to 500 × 500 × 500 μm^3. Following the removal of the DMF guests by evacuation at elevated temperatures, the crystals obtain a large number of cracks and turn opaque (*dry*-MOF-5-**C6**). After re-infiltration of *n*-octane, the crystals again turn transparent (*oct*-MOF-5-**C6**), even though some of the cracks remain. Reconstructed reciprocal space sections of the (*hk*0) plane calculated from the raw data of previously published single-crystal x-ray diffraction data of *as*-, *dry*-, and *oct*-MOF-5-**C6**[38] nicely illustrate the structural changes as well [Fig. 3(b)]. *as*-MOF-5-**C6** crystallizes in the cubic space group $Pm\bar{3}m$ (a = 12.9040(12) Å, V = 2148.7(6) $Å^3$, and V/Z = 2148.7(6) $Å^3$; Z = the number of formula units per unit cell) and features the typical cubic diffraction pattern of MOF-5-type materials with strong Bragg peaks. Interestingly, the reciprocal space map of *dry*-MOF-5-**C6** shows weak Bragg features of the formerly cubic diffraction pattern of *as*-MOF-5-**C6**, but also extensive diffuse scattering signatures originating from the aperiodic structural distortions, thus highlighting the disordered semi-crystalline nature of the guest-free MOF.

Following inclusion of the *n*-octane guest molecules (*oct*-MOF-5-**C6**), the crystals recover high crystallinity but adopt a different cubic structure compared to *as*-MOF-5-**C6**, evidenced by additional superstructure reflections [Fig. 3(b)]. The structure of *oct*-MOF-5-**C6** is described in the primitive cubic space group $Pa\bar{3}$ with a = 25.7145(6) Å [Fig. 4(a), V = 17003.3(12) $Å^3$, and V/Z = 2125.4(2) $Å^3$, 98.5% of V/Z of *as*-MOF-5-**C6**] and, thus, slightly contracted compared to the original DMF-containing MOF. In contrast to the DMF-containing MOF, the **C6**-alkyl sidechains could be resolved in the electron density map of *oct*-MOF-5-**C6**, revealing their arrangement on the faces of the pseudo-cubic cavities. The interior of each MOF cavity features a volume of about 580 $Å^3$ (amounting to 27% of the crystal volume) that is filled with disordered *n*-octane molecules [Fig. 4(b)]. By taking the central O^{2-} ions of the $Zn_4O(CO_2)_6$ units as six-connecting vertices, the structure

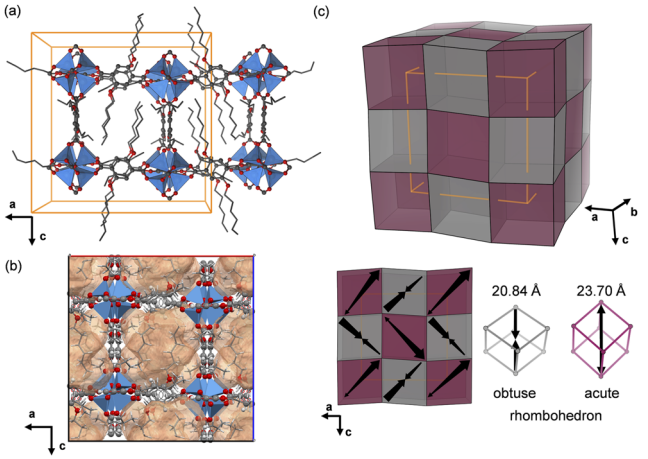

FIG. 4. (a) Crystal structure of *oct*-MOF-5-**C6** (space group $Pa\bar{3}$; CCDC deposition code 2 -040 -925) with unit cell edges marked in orange color. The twofold disorder of the $[Zn_4O(O_2C)_6]$ units and the alkyl chains was removed for clarity. The atom color code is identical to Fig. 1(a). (b) View of the crystal structure of *oct*-MOF-5-**C6** showing the voids occupied by *n*-octane. The void volume amounts to 27% of the crystal volume and was determined with the program Mercury applying a probe size of 1.5 Å and a grid spacing of 0.2 Å. The twofold disorder of some atoms has been resolved in order to obtain a reasonable void volume. (c) Simplified representations of the structure of *oct*-MOF-5-**C6** showcasing the alternating arrangement of acute (magenta) and obtuse (gray) rhombohedral cavities (i.e., the volume of one $[Zn_4O(\mathbf{C6}\text{-bdc})_3]$ repeating unit). The arrows inserted in the front view indicate the rhombohedral elongation (acute rhombohedra) or contraction (obtuse rhombohedra) axes.

of *oct*-MOF-5-**C6** can be understood as an arrangement of alternating acute and obtuse rhombohedral MOF cavities [Fig. 4(c)], which are constructed of the very same rhombic faces. The angles of the rhombohedra amount to 86.33° and 93.67°, emphasizing a significant deviation from the original cubic cavities of *as*-MOF-**C6** (naturally possessing an angle of 90°). This highlights that *oct*-MOF-5-**C6** features two different types of rhombohedrally distorted MOF cavities, which globally arrange in a cubic structure. This is in contrast to the other rhombohedrally distorted derivatives of MOF-5-**CX** with longer alkyl chains that feature global rhombohedral symmetry (i.e., all cavities are acute rhombohedra arranging in a rhombohedral crystal structure with $R\bar{3}$ symmetry, as, for example, in *dry*-MOF-5-**C7**).[38] Ultimately, the $Pa\bar{3}$ structure of *oct*-MOF-5-**C6** can be interpreted as an intermediate between the fully expanded *as*-MOF-5-**C6** and the contracted semi-crystalline *dry*-MOF-5-**C6**. This is explained as follows when considering the thermal behavior of *dry*-MOF-5-**C6**.

Structural response to temperature

With this new understanding of the crystal structure of *oct*-MOF-5-**C6** at hand, we now reanalyze the VT-PXRD patterns of *dry*-MOF-5-**C6** previously recorded between 300 and 500 K [Fig. 5(a)].[38] Evidently, *dry*-MOF-5-**C6** is poorly crystalline at 300 K, displaying very broad reflections with an anisotropic peak shape. Upon heating the material to 500 K, the absolute intensity of the reflections progressively increases, while the reflections significantly sharpen and shift to lower Q values. Previous experiments already indicated that the transition from the semi-crystalline to the crystalline state is continuous as no signal is observed in differential scanning calorimetry.[38] The unprecedented increase in crystallinity and scattering intensity with increasing temperature disagrees with the established temperature-dependent dampening of the x-ray scattering factors due to thermal vibrations according to Debye and Waller.[42,43] Remarkably, the diffraction pattern of *dry*-MOF-5-**C6** recorded at 500 K can be indexed in the space group $Pa\bar{3}$ (analogous to *oct*-MOF-5-**C6**) as established by a structureless profile refinement [using the Pawley method;[44] Fig. 5(b)], giving a unit cell parameter a = 25.716(14) Å and a reduced unit cell volume V/Z = 2126(3) Å^3. The validity of $Pa\bar{3}$ symmetry is also confirmed by the weak reflection at $Q \approx 0.55$ Å^{-1}, which would be absent in the fully expanded structure with $Pm\bar{3}m$ symmetry but can be indexed

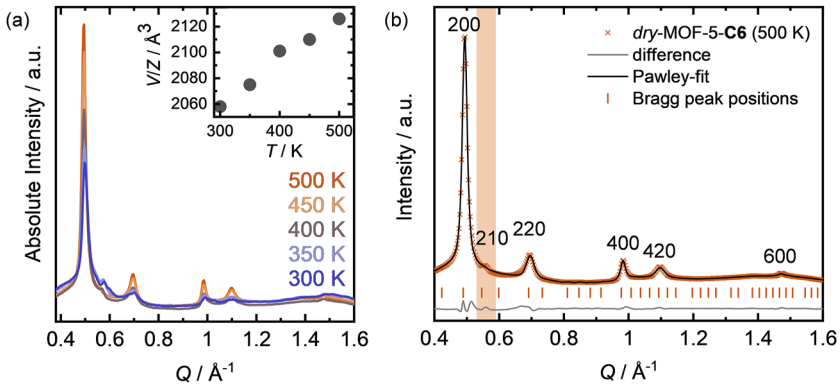

FIG. 5. (a) VT-PXRD data of *dry*-MOF-5-**C6** (collected at P02.1 of DESY, λ = 0.2073 Å) in the range from 300 to 500 K.[38] The inset shows the progression of the reduced unit cell volume (V/Z) derived from profile fits applying cubic symmetry (space group $Pa\bar{3}$ as for *oct*-MOF-5-**C6**) and the Stephens model for anisotropic strain broadening. (b) Representative profile fit to the PXRD pattern of *dry*-MOF-5-**C6** recorded at 500 K [lattice parameter a = 25.716(14) Å, space group $Pa\bar{3}$; see Table S2 for further parameters]. The Laue indices *hkl* of selected reflections are given. The weak 210 reflection in the highlighted region between Q = 0.53 and 0.58 Å^{-1} supports the presence of $Pa\bar{3}$ symmetry.

as the 210 reflection in $Pa\bar{3}$ [see Fig. 5(b), highlighted region]. Nevertheless, *dry*-MOF-5-**C6** still appears to contain a significant anisotropic strain at 500 K, which is apparent from large variations in the peak width between reflections of the *h*00 and *hk*0 families. We modeled the anisotropic strain broadening of the reflections using the method reported by Stephens[45] (see the supplementary material) and derived the strain parameters S_{400} and S_{220}, which quantify the microstrain of the sample along the crystallographic [100] and [110] directions, respectively. Importantly, S_{220} is more than an order of magnitude larger than S_{400}, indicating a cubic MOF structure with local rhombohedral distortions of varying magnitudes. Based on these results, we moved on and also fitted the PXRD patterns recorded at lower temperatures by also applying $Pa\bar{3}$ symmetry and the Stephens model for anisotropic strain broadening. With decreasing temperature, poorer fits to the PXRD patterns are obtained, indicating significant deviations from cubic symmetry, particularly below 400 K (Fig. S3). This is also manifested in strongly increasing strain parameters (especially S_{220}) at lower temperatures (Table S2). Nevertheless, the fits allow extracting the cubic lattice parameter (*a*) and the corresponding reduced unit cell volume (*V*/*Z*) for all temperatures investigated. *V*/*Z* monotonically increases by about 3% when *dry*-MOF-5-**C6** is heated from 300 to 500 K [Fig. 5(a), inset], highlighting that the thermal expansion of the aperiodically distorted *dry*-MOF-5-**C6** leads to a reduction in the microstrain and significantly increased crystallinity at high temperatures.

Based on the new insights into the *global* structural changes of *dry*-MOF-5-**C6** as a function of temperature, we used VT x-ray total scattering and VT-FTIR spectroscopy to investigate the changes of the *local* structure with the aim of better understanding the microscopic mechanism of the material's thermo-responsive behavior. XPDFs calculated from the VT x-ray total scattering data indicate an increase in the long-range correlations within the material when heating from 300 to 525 K [Fig. 6(a); see Fig. S4 for the corresponding *S*(*Q*) data]. This is evident from the sharpening of the peaks at 18–20 Å, corresponding to Zn···Zn distances across the face and space diagonals of the distorted pseudo-cubic cavities of the MOF. More importantly, the emerging peak at $r \approx 41$ Å, corresponding to Zn···Zn distances across the space diagonal spanning two MOF cavities, clearly establishes increased long-range order with increasing temperature. On the contrary, we could not detect significant changes in the low *r* regions of the PDFs with temperature, also for the prominent peaks for the Zn–O (peak **A**) and Zn–Zn distances (peak **B**) of the $[Zn_4O(O_2C)_6]$ cluster.

VT-FTIR spectroscopy experiments recorded in the range from 300 to 525 K provide information on the temperature-driven structural changes of the inorganic building unit, as well as the dangling **C6**-alkyl sidechains [Fig. 6(b), S5, and S6]. The asymmetric stretching vibration of the $[Zn_4O]^{6+}$ cluster (ν_{as}(Zn–O1), O1 corresponds to the central O^{2-} ion of the cluster) located around 510 cm^{-1} is sensitive toward the reduction in the symmetry of the $[Zn_4O(O_2C)_6]$ building unit.[46] Hence, this band appears visibly broadened in the aperiodically contracted *dry*-MOF-5-**C6** at 300 K, suggesting a distribution of differently distorted inorganic building units at this temperature. Upon heating the material to 525 K, this band continuously becomes sharper, establishing the recovery of T_d symmetry and more structural homogeneity among the $[Zn_4O(O_2C)_6]$ units with increasing temperature. In line with this, the asymmetric

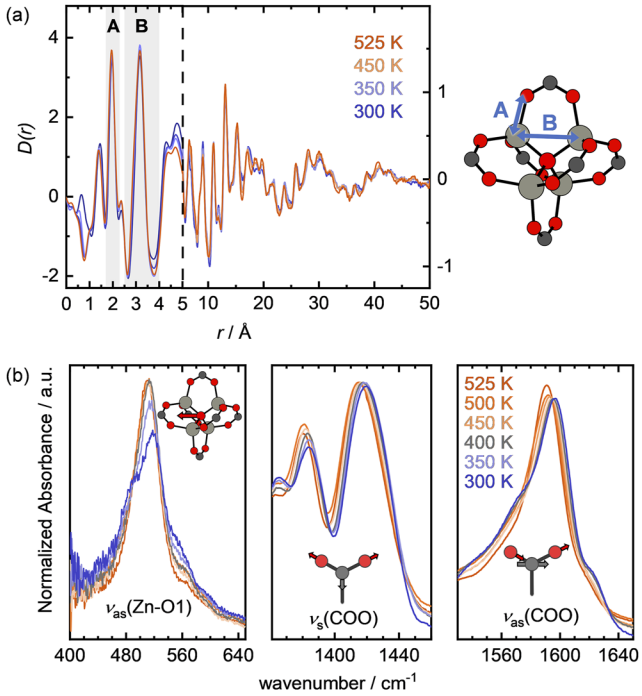

FIG. 6. (a) VT-XPDFs of *dry*-MOF-5-**C6** along with a representation of the $[Zn_4O(O_2C)_6]$ cluster with prominent short-range atom–atom distances highlighted. Zn, O, and C atoms are shown in light gray, red, and dark gray, respectively. Note that the XPDF data are scaled differently from $r = 5$ Å onward to enhance the visibility of the short-range region. (b) Excerpts of the VT-FTIR spectra of *dry*-MOF-5-**C6** recorded in the range from 300 to 525 K showing the asymmetric Zn–O1, as well as the symmetric and the asymmetric carboxylate stretching vibrations.

carboxylate stretching vibration [ν_{as}(COO)] at around 1590 cm^{-1} also exhibits a slight sharpening and disappearance of shoulders associated with this band, thus signifying less distorted states and higher homogeneity among the inorganic building units at elevated temperatures. Interestingly, ν_{as}(COO) displays a redshift of the band maximum from 1597 cm^{-1} (300 K) to 1591 cm^{-1} (525 K), which likewise is observable for the symmetric carboxylate stretching vibration [ν_s(COO)] located at around 1420 cm^{-1}. This phenomenon has been ascribed to an increasing population of a more "loose" state of the carboxylate-to-metal coordination along with the depopulation of a "tight" state with increasing temperature.[47] This weakening of the Zn–O(carboxylate) bonds could also facilitate the recovery of time-averaged T_d symmetry of the $[Zn_4O(O_2C)_6]$ units.

While the vibrational bands ν_{as}(Zn–O1), ν_s(COO), and ν_{as}(COO) become sharper and more intense with increasing temperature, the bands in the spectral region between 700 and 900 cm^{-1} undergo a significant loss in intensity and exhibit band broadening of varying magnitudes (Fig. 7). This region contains vibrational bands corresponding to CH_2-rocking modes, which are particularly sensitive to conformational changes of alkyl chains (i.e., *trans*, *gauche*, and their combinations) but also to their local

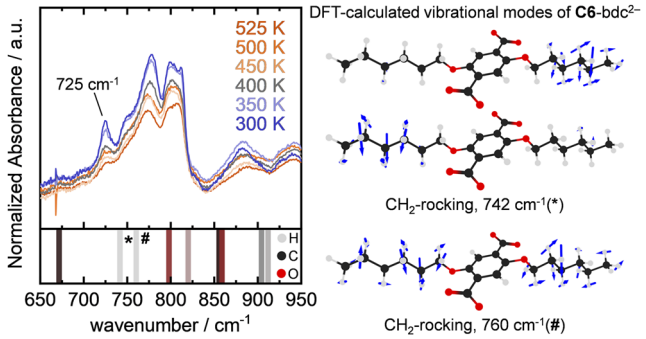

FIG. 7. Excerpt of the VT-FTIR spectra of *dry*-MOF-5-**C6** from 650 to 950 cm^{-1} with simulated IR band maxima of the **C6**-bdc^{2-} linker obtained from DFT calculations. The simulated band maxima are colored depending on the degree of contribution of certain atom species (H, C, or O atoms) to the IR active modes. Depicted on the right are visualizations of vibrational modes corresponding to CH_2-rocking modes of the alkyl chains of **C6**-bdc^{2-}. The CH_2-rocking mode appearing at 742 cm^{-1} is double degenerate.

environment.[48–52] In order to aid the assignment of the experimentally observed vibrational bands, theoretical IR absorption spectra of the free **C6**-bdc^{2-} linker were computed by density functional theory (DFT) calculations (see the supplementary material). According to the calculated normal modes of the linker, the vibrational band located at 725 cm^{-1} in the experimental FTIR spectra is assigned to the CH_2-rocking vibrations of the **C6**-alkyl sidechains. Similarly, the weak band shoulder appearing at 748 cm^{-1} also refers to CH_2-rocking vibrations of the **C6**-alkyl substituents. On the contrary, the broad and overlapping vibrational bands in the range from 760 to 830 cm^{-1} are assigned to modes containing significant contributions from bending vibrations of the aromatic ring and the carboxylate groups (see the supplementary material, Fig. S7).

The almost complete disappearance of the CH_2-rocking band at 725 cm^{-1} upon heating from 300 to 525 K is interesting, since a similar intensity decrease of this mode is known to happen upon melting of long-chain *n*-alkanes or polyethylene.[50,52,53] Thus, we conclude that the **C6**-alkyl chains possess rather fixed conformations at 300 K, most likely due to attractive dispersion interactions with the framework backbone and among themselves. With increasing temperature, however, the framework expands and the **C6**-alkyl chains gain not only vibrational but also rotational degrees of freedom along the axes of the C–C bonds, giving rise to a larger number of different alkyl chain conformers. This results in the superposition of the CH_2-rocking modes of the individual conformers and the de-facto blending of this band into the baseline of the spectrum. Similarly, this is in line with the overall decrease in band intensity observable in the spectral region from about 710 to 830 cm^{-1} since the computed IR spectrum of the **C6**-bdc^{2-} linker indicates contributions from CH_2-rocking to almost all vibrational bands located in this region (see Fig. S7 for visualizations of the corresponding IR modes). Unfortunately, these IR bands, except the one appearing at 725 cm^{-1}, suffer from significant overlapping, rendering a more detailed analysis and extraction of information of conformational changes of the **C6**-alkyl groups with increasing temperature very difficult. Nevertheless, the VT-FTIR data, for the first time, establish that the thermally induced relaxation of the framework backbone of *dry*-MOF-5-**C6** to the crystallographically more ordered cubic phase is accompanied by a "melting-like" change of the flexible **C6**-alkyl chains. The increased vibrational and conformational disorder of the **C6**-alkyl chains inevitably contributes to the weakening of intra-framework dispersion interactions of the alkyl chains. Thus, increasing the temperature generates higher disorder of the **C6**-alkyl chains, which, in turn, forces the inorganic building units of the material to relax on a cubic lattice. In a thermodynamic picture, the increased vibrational and conformational entropies of the **C6**-alkyl chains at elevated temperatures outbalance the increased crystallographic order (and, thus, lower entropy) of the framework backbone.

CONCLUSION

We investigated the structural phase behavior of a hexyloxy-functionalized MOF-5 derivative, MOF-5-**C6**, in detail. This material switches between an expanded cubic crystalline phase and a contracted semi-crystalline phase as a function of guest content and temperature. The unusual responsive behavior is driven by attractive dispersion interactions of the alkoxy groups with the framework backbone and among themselves, stabilizing the contracted semi-crystalline phase in the guest-free state at room temperature. Herein, we analyzed the surprising structure of the *n*-octane-solvated phase *oct*-MOF-5-**C6**, which features a slightly contracted framework via the formation of alternating obtuse and acute rhombohedral cavities. This structure bears relevance for the more drastic aperiodic structural distortions apparent in the guest-free semi-crystalline *dry*-MOF-5-**C6**. This is supported via a detailed analysis of VT-PXRD patterns by accounting for the presence of a large anisotropic strain. With increasing temperature, the strain in *dry*-MOF-5-**C6** is partially released and the structure relaxes toward the fully expanded cubic state. VT-FTIR data provide evidence that the temperature-induced increase in crystallinity, indeed, comes along with a recovery of the T_d symmetry of the $[Zn_4O(O_2C)_6]$ nodes of the material, while thermally excited vibrations of the alkoxy groups drive the transformation by overcoming intra-framework dispersion interactions.

Fundamentally, our results demonstrate how a chemically simple framework modification along the principles of isoreticular chemistry[54] can create highly complex stimuli-responsive phase behaviors in otherwise structurally rigid and non-responsive MOFs. The thermal control over non-correlated distortions of the inorganic framework building units presented here is potentially useful for systematically tuning the catalytic or optoelectronic properties of MOFs.

DEDICATION

Dedicated to Professor Sir Tony Cheetham on the occasion of his 75th birthday.

SUPPLEMENTARY MATERIAL

Additional PXRD patterns and refinement data, x-ray total scattering functions, complete VT-FTIR spectra, and further information regarding the simulated IR spectra are given in the supplementary material file.

ACKNOWLEDGMENTS

We acknowledge Diamond Light Source (DLS) for access to beamline I15-1 (Grant No. EE15895-1), which contributed to the results presented here. Beamline scientist Philip Chater is thanked for his support with the x-ray total scattering experiments at DLS. We thank Louis Frentzel-Beyme for his help in the collection of data at DLS. We acknowledge DESY (Hamburg, Germany), a member of the Helmholtz Association HGF, for the provision of experimental facilities. Parts of this research were carried out at PETRA III on beamline P02.1 (Experiment No. I-20180709). We further thank Michael T. Wharmby for his support with the VT-PXRD experiments and Louis Frentzel-Beyme, Andrea Machalica, and Marvin Kloβ for their help in the collection of the VT-PXRD data. We acknowledge financial support by Deutsche Forschungsgemeinschaft and Technische Universität Dortmund/TU Dortmund University within the funding programme Open Access Costs.

AUTHOR DECLARATIONS

Conflict of Interest

The authors have no conflicts to disclose.

Author Contributions

Roman Pallach: Conceptualization (equal); Data curation (lead); Formal analysis (lead); Investigation (lead); Methodology (lead); Validation (equal); Visualization (lead); Writing – original draft (lead); Writing – review & editing (equal). **Jan-Benedikt Weiß**: Data curation (equal); Formal analysis (equal); Investigation (equal). **Katrin Vollmari**: Investigation (equal); Methodology (equal). **Sebastian Henke**: Conceptualization (equal); Funding acquisition (lead); Project administration (lead); Resources (lead); Supervision (lead); Validation (equal); Writing – review & editing (equal).

DATA AVAILABILITY

The data that support the findings of this study are available within the article and its supplementary material. The raw data are available from the corresponding author upon reasonable request.

REFERENCES

[1] H. Furukawa, K. E. Cordova, M. O'Keeffe, and O. M. Yaghi, Science **341**, 1230444 (2013).
[2] L. Jiao, J. Y. R. Seow, W. S. Skinner, Z. U. Wang, and H.-L. Jiang, Mater. Today **27**, 43 (2019).
[3] A. Schneemann, V. Bon, I. Schwedler, I. Senkovska, S. Kaskel, and R. A. Fischer, Chem. Soc. Rev. **43**, 6062 (2014).
[4] Y. Liu, J.-H. Her, A. Dailly, A. J. Ramirez-Cuesta, D. A. Neumann, and C. M. Brown, J. Am. Chem. Soc. **130**, 11813 (2008).
[5] Q. Zeng, K. Wang, and B. Zou, J. Am. Chem. Soc. **139**, 15648 (2017).
[6] P. Serra-Crespo, A. Dikhtiarenko, E. Stavitski, J. Juan-Alcañiz, F. Kapteijn, F.-X. Coudert, and J. Gascon, CrystEngComm **17**, 276 (2015).
[7] A. P. Katsoulidis, D. Antypov, G. F. S. Whitehead, E. J. Carrington, D. J. Adams, N. G. Berry, G. R. Darling, M. S. Dyer, and M. J. Rosseinsky, Nature **565**, 213 (2019).
[8] F. Salles, G. Maurin, C. Serre, P. L. Llewellyn, C. Knöfel, H. J. Choi, Y. Filinchuk, L. Oliviero, A. Vimont, J. R. Long, and G. Férey, J. Am. Chem. Soc. **132**, 13782 (2010).
[9] N. Yanai, T. Uemura, M. Inoue, R. Matsuda, T. Fukushima, M. Tsujimoto, S. Isoda, and S. Kitagawa, J. Am. Chem. Soc. **134**, 4501 (2012).
[10] A. Ghoufi, K. Benhamed, L. Boukli-Hacene, and G. Maurin, ACS Cent. Sci. **3**, 394 (2017).
[11] A. Knebel, B. Geppert, K. Volgmann, D. I. Kolokolov, A. G. Stepanov, J. Twiefel, P. Heitjans, D. Volkmer, and J. Caro, Science **358**, 347 (2017).
[12] B. E. R. Snyder, A. B. Turkiewicz, H. Furukawa, M. V. Paley, E. O. Velasquez, M. N. Dods, and J. R. Long, Nature **613**, 287 (2023).
[13] Y. Su, K.-i. Otake, J.-J. Zheng, S. Horike, S. Kitagawa, and C. Gu, Nature **611**, 289 (2022).
[14] N. Yanai, K. Kitayama, Y. Hijikata, H. Sato, R. Matsuda, Y. Kubota, M. Takata, M. Mizuno, T. Uemura, and S. Kitagawa, Nat. Mater. **10**, 787 (2011).
[15] L. E. Kreno, K. Leong, O. K. Farha, M. Allendorf, R. P. Van Duyne, and J. T. Hupp, Chem. Rev. **112**, 1105 (2012).
[16] P. G. Yot, L. Vanduyfhuys, E. Alvarez, J. Rodriguez, J.-P. Itié, P. Fabry, N. Guillou, T. Devic, I. Beurroies, P. L. Llewellyn, V. Van Speybroeck, C. Serre, and G. Maurin, Chem. Sci. **7**, 446 (2016).
[17] J. Fonseca, T. Gong, L. Jiao, and H.-L. Jiang, J. Mater. Chem. A **9**, 10562 (2021).
[18] T. D. Bennett, F.-X. Coudert, S. L. James, and A. I. Cooper, Nat. Mater. **20**, 1179 (2021).
[19] S. Kitagawa, Acc. Chem. Res. **50**, 514 (2017).
[20] M.-S. Yao, K.-i. Otake, Z.-Q. Xue, and S. Kitagawa, Faraday Discuss. **231**, 397 (2021).
[21] A. Simonov and A. L. Goodwin, Nat. Rev. Chem. **4**, 657 (2020).
[22] T. D. Bennett and A. K. Cheetham, Acc. Chem. Res. **47**, 1555 (2014).
[23] T. D. Bennett and S. Horike, Nat. Rev. Mater. **3**, 431 (2018).
[24] T. D. Bennett, A. K. Cheetham, A. H. Fuchs, and F.-X. Coudert, Nat. Chem. **9**, 11 (2016).
[25] S. Horike, S. S. Nagarkar, T. Ogawa, and S. Kitagawa, Angew. Chem., Int. Ed. **59**, 6652 (2020).
[26] N. Castel and F.-X. Coudert, J. Phys. Chem. C **126**, 6905 (2022).
[27] N. Ma and S. Horike, Chem. Rev. **122**, 4163 (2022).
[28] S. Li, R. Limbach, L. Longley, A. A. Shirzadi, J. C. Walmsley, D. N. Johnstone, P. A. Midgley, L. Wondraczek, and T. D. Bennett, J. Am. Chem. Soc. **141**, 1027 (2019).
[29] A. Dhakshinamoorthy, M. Alvaro, P. Horcajada, E. Gibson, M. Vishnuvarthan, A. Vimont, J.-M. Grenèche, C. Serre, M. Daturi, and H. Garcia, ACS Catal. **2**, 2060 (2012).
[30] C. Liu, J. Wang, J. Wan, Y. Cheng, R. Huang, C. Zhang, W. Hu, G. Wei, and C. Yu, Angew. Chem., Int. Ed. **59**, 3630 (2020).
[31] L. Jiao and H.-L. Jiang, Chin. J. Catal. **45**, 1 (2023).
[32] A. F. Sapnik, C. W. Ashling, L. K. Macreadie, S. J. Lee, T. Johnson, S. G. Telfer, and T. D. Bennett, J. Mater. Chem. A **9**, 27019 (2021).
[33] L. Frentzel-Beyme, P. Kolodzeiski, J.-B. Weiß, A. Schneemann, and S. Henke, Nat. Commun. **13**, 7750 (2022).
[34] C. Orellana-Tavra, R. J. Marshall, E. F. Baxter, I. A. Lázaro, A. Tao, A. K. Cheetham, R. S. Forgan, and D. Fairen-Jimenez, J. Mater. Chem. B **4**, 7697 (2016).
[35] X. Wu, H. Yue, Y. Zhang, X. Gao, X. Li, L. Wang, Y. Cao, M. Hou, H. An, L. Zhang, S. Li, J. Ma, H. Lin, Y. Fu, H. Gu, W. Lou, W. Wei, R. N. Zare, and J. Ge, Nat. Commun. **10**, 5165 (2019).

[36]B. Bueken, F. Vermoortele, M. J. Cliffe, M. T. Wharmby, D. Foucher, J. Wieme, L. Vanduyfhuys, C. Martineau, N. Stock, F. Taulelle, V. Van Speybroeck, A. L. Goodwin, and D. De Vos, Chem. - Eur. J. **22**, 3264 (2016).
[37]J.-W. Xiu, G.-E. Wang, M.-S. Yao, C.-C. Yang, C.-H. Lin, and G. Xu, Chem. Commun. **53**, 2479 (2017).
[38]R. Pallach, J. Keupp, K. Terlinden, L. Frentzel-Beyme, M. Kloß, A. Machalica, J. Kotschy, S. K. Vasa, P. A. Chater, C. Sternemann, M. T. Wharmby, R. Linser, R. Schmid, and S. Henke, Nat. Commun. **12**, 4097 (2021).
[39]G. Férey and C. Serre, Chem. Soc. Rev. **38**, 1380 (2009).
[40]L. Sarkisov, R. L. Martin, M. Haranczyk, and B. Smit, J. Am. Chem. Soc. **136**, 2228 (2014).
[41]H. Li, M. Eddaoudi, M. O'Keeffe, and O. M. Yaghi, Nature **402**, 276 (1999).
[42]P. Debye, Ann. Phys. **348**, 49 (1913).
[43]I. Waller, Z. Phys. **17**, 398 (1923).
[44]G. S. Pawley, J. Appl. Crystallogr. **14**, 357 (1981).
[45]P. W. Stephens, J. Appl. Crystallogr. **32**, 281 (1999).
[46]B. Civalleri, F. Napoli, Y. Noël, C. Roetti, and R. Dovesi, CrystEngComm **8**, 364 (2006).
[47]A. B. Andreeva, K. N. Le, L. Chen, M. E. Kellman, C. H. Hendon, C. K. Brozek, and C. H. Hendon, J. Am. Chem. Soc. **142**, 19291 (2020).
[48]R. G. Snyder, J. Chem. Phys. **47**, 1316 (1967).
[49]R. G. Snyder, M. Maroncelli, S. P. Qi, and H. L. Strauss, Science **214**, 188 (1981).
[50]G. Zerbi, R. Magni, M. Gussoni, K. H. Moritz, A. Bigotto, and S. Dirlikov, J. Chem. Phys. **75**, 3175 (1981).
[51]R. G. Snyder and M. W. Poore, Macromolecules **6**, 708 (1973).
[52]V. A. Marikhin, L. P. Myasnikova, E. I. Radovanova, B. Z. Volchek, and D. A. Medvedeva, Phys. Solid State **59**, 331 (2017).
[53]K. Tashiro, S. Sasaki, and M. Kobayashi, Macromolecules **29**, 7460 (1996).
[54]R. Freund, S. Canossa, S. M. Cohen, W. Yan, H. Deng, V. Guillerm, M. Eddaoudi, D. G. Madden, D. Fairen-Jimenez, H. Lyu, L. K. Macreadie, Z. Ji, Y. Zhang, B. Wang, F. Haase, C. Wöll, O. Zaremba, J. Andreo, S. Wuttke, and C. S. Diercks, Angew. Chem., Int. Ed. **60**, 23946 (2021).